Contact inhibition of locomotion determines cell–cell and cell–substrate forces in tissues

Juliane Zimmermann[a], Brian A. Camley[b], Wouter-Jan Rappel[b], and Herbert Levine[a,1]

[a]Center for Theoretical Biological Physics, Rice University, Houston, TX 77005; and [b]Department of Physics, University of California, San Diego, La Jolla, CA 92093

Contributed by Herbert Levine, January 20, 2016 (sent for review November 12, 2015; reviewed by Vincent Hakim and Andre Levchenko)

Cells organized in tissues exert forces on their neighbors and their environment. Those cellular forces determine tissue homeostasis as well as reorganization during embryonic development and wound healing. To understand how cellular forces are generated and how they can influence the tissue state, we develop a particle-based simulation model for adhesive cell clusters and monolayers. Cells are contractile, exert forces on their substrate and on each other, and interact through contact inhibition of locomotion (CIL), meaning that cell–cell contacts suppress force transduction to the substrate and propulsion forces align away from neighbors. Our model captures the traction force patterns of small clusters of nonmotile cells and larger sheets of motile Madin–Darby canine kidney (MDCK) cells. In agreement with observations in a spreading MDCK colony, the cell density in the center increases as cells divide and the tissue grows. A feedback between cell density, CIL, and cell–cell adhesion gives rise to a linear relationship between cell density and intercellular tensile stress and forces the tissue into a nonmotile state characterized by a broad distribution of traction forces. Our model also captures the experimentally observed tissue flow around circular obstacles, and CIL accounts for traction forces at the edge.

contact inhibition | tissue mechanics | collective motility

To move during morphogenesis, tissue repair, and cancer metastasis, cells exert forces on their extracellular environment and neighboring cells. Understanding how cellular forces are generated is vital for understanding those physiologically relevant processes. More than a decade ago, traction force microscopy was developed to measure the forces that single spreading or migrating cells exert on their substratum, and it has since then been refined and applied to different cell types under various conditions (1–4). In single cells, forces predominantly arise from active contractions of the cytoskeleton, which are balanced by forces on the substrate at adhesion sites, as well as lamellipodial protrusion forces in migrating cells (5).

More recently, interest has shifted toward deciphering the forces that multiple cells that are adhered to each other, in either small clusters (6–11) or larger sheets (12–17), exert on a substrate. Because of interaction with their neighbors, cells in a tissue can behave significantly different from single cells. In particular, substrate forces exerted by single cells are always balanced (7), meaning that the vector sum of traction forces is zero, because inertial forces and friction with the surrounding fluid are negligible. A cell in a tissue, however, can have imbalanced substrate forces that are balanced by forces on cell–cell adhesions (7). Such a behavior is observed with clusters of 2 to about 30 nonmotile keratinocytes (8, 9) and motile Madin–Darby canine kidney (MDCK) (7) and MCF10A breast epithelial (10) cells. Interestingly, those clusters develop a substrate force pattern that strikingly resembles the force pattern of a single cell, with strong inward directed forces exerted at the edge and only weak forces exerted by cells in the interior. This observation has led to the notion of adhesive clusters forming a "supercell"; however, the mechanism leading to weaker substrate forces at sites of cell–cell adhesion is not understood.

The situation is even more complex for large spreading tissues of several thousand collectively migrating MDCK cells (13). Although cells at the edge still exert the strongest forces on the substrate, forces exerted by cells throughout the tissue are nonnegligible, leading to a very heterogeneous traction force pattern. Traction stresses of single cells in the tissue are unbalanced, and the net traction forces are, on average, directed toward the center of the spreading circular tissue. In other words, the direction of imbalanced traction stresses in the tissue interior correlates with the direction of traction stresses at the edge. This correlation implies that stresses on cell–cell adhesions increase toward the interior. Despite the strong pulling forces that cells exert on each other at the center of the tissue, the cell density is highest there and proportional to the tensile stress on cell–cell adhesions (13). The direction of traction force does not, however, necessarily correlate with the direction of motion, which is the case in the expanding circular colony. This fact was shown in a different experiment, where cells move around a circular "obstacle" consisting of uncoated substrate area (16). The cell sheet moves toward the obstacle, splits on contact, and rejoins at the back, whereas the cells maintain their general direction of migration, reminiscent of a fluid flowing around a cylinder. Substrate forces, however, are always directed away from the obstacle center and toward the tissue interior, leading to contrary alignments between traction force and velocity vectors at the "upstream and downstream stagnation points" (16).

The collective cell migration of tissue reorganization and wound healing has been subject to extensive mathematical modeling. In particular, continuum models that describe the tissue as an elastic material were successful in reproducing the stress buildup toward the center of a spreading tissue when cells migrate outward (18, 19). However, those macroscopic models cannot provide a conclusive description of how cells generate forces, align, divide, and maintain tissue integrity on an individual cell level. Cellular Potts or vertex models (20–22), phase field models (23–25), and particle models (26–29) use a bottom-up approach instead and focus on individual cell properties. However, these models were mainly used to explore cellular flow patterns and tissue morphologies, and they

Significance

Many cell types organize into tissues (e.g., in the skin). In most adult tissues, cells are tightly anchored and attached to each other through intercellular adhesions. However, during embryonic development and wound repair, cells reorganize and migrate to (re)establish the desired tissue shape. This reorganization involves a complex interplay of cell motility, cell contractility, and cell–cell adhesion. Here, we use a computational model to study the forces generated by cells in tissues and the resultant cell motion. A basic hypothesis, namely that cell–cell contacts repolarize moving cells and suppress their ability to exert forces on the environment, allows us to explain heretofore surprising findings showing that tissues are under tension and that this tension increases with cell density.

Author contributions: J.Z., W.-J.R., and H.L. designed research; J.Z., B.A.C., W.-J.R., and H.L. performed research; J.Z., B.A.C., and W.-J.R. analyzed data; and J.Z. and H.L. wrote the paper.

Reviewers: V.H., Ecole Normale Superieure; and A.L., Yale University.

The authors declare no conflict of interest.

[1]To whom correspondence should be addressed. Email: herbert.levine@rice.edu.

This article contains supporting information online at www.pnas.org/lookup/suppl/doi:10.1073/pnas.1522330113/-/DCSupplemental.

do not explain how substrate forces and intercellular stresses are generated in cell colonies. The particle model by Basan et al. (27) is, to our knowledge, the only microscopic model that predicts not only velocity but also force patterns. In this model, spreading cell colonies are initially under tension, in agreement with the experimental data; however, as the colony grows and the tissue density increases, cells exert increasing pressure on each other (27). Consequently, the model does not reproduce the linear relationship between cell density and tension (13). Traction forces in this model are caused by "motility forces" that moving cells exert on the substrate (27). Therefore, nonmotile cells do not exert forces on a substrate at all (30), contrary to experimental observations (8). Moreover, motility forces align with cellular velocities in the model (27). Hence, it cannot explain the traction force pattern of cells moving around an obstacle, where a counteralignment between traction forces and velocities is observed at the downstream stagnation point (16).

In this article, we address those previously unexplained effects using a more advanced particle-based simulation model for collective cell migration. In our model, both nonmotile and motile cells exert traction forces on a substrate to balance intracellular contraction. Our model cells adhere to each other, and cell–cell contact weakens forces on the substrate. Furthermore, substrate forces tend to align perpendicular to a tissue boundary. A similar effect was observed for clusters of motile cells and is referred to as "contact inhibition of locomotion" (CIL), generally meaning that contact with other cells suppresses the formation of lamellipodia, such that cells tend to move away from each other (31–35). Active cell to cell signaling mediates CIL in those cases. On a molecular level, contact with another cell is sensed by membrane receptors (e.g., through ephrin signaling) and integrated into the small Rho-GTPases signaling network that determines formation of lamellipodia and cell polarity (36). However, downstream effectors can vary in different cell types (34). In neural crest cells and some cancer cells, RhoA is activated, leading to retraction and motion of both cells in opposite directions (37, 38). In contrast, Eph receptor signaling inhibits lamellipodial protrusion through inhibiting Rac upstream of PI3K in MTLn3 breast cancer cells (34). In the context of a spreading tissue, the tendency of cells to align away from the bulk to invade empty space was termed "kenotaxis" (16), without the specification of a subcellular mechanism. We hypothesize that a similar effect also leads to supercell formation in clusters of nonmotile cells and even in this case, denote the interaction between the presence of neighboring cells and substrate forces as CIL, although it is not quite accurate for nonmotile cells, which do not "locomote." In those clusters, polarization of cells at the edge is possibly initiated by cadherin signaling (9, 39). We do not further specify the molecular mechanism for CIL in our model—it could be caused by mechanical interaction between the cells or an exchange of signaling molecules (36, 40). However, CIL is represented by a short-range interaction—only close neighbors influence substrate forces of a cell. Our model uses a mechanism where either Rac-mediated lamellipodial protrusion or adhesion with the substrate is impaired by the presence of neighboring cells rather than CIL having an impact on intracellular contraction. As a consequence, cells tend to move away from their neighbors, and their motility forces are decreased by the presence of their neighbors.

Our model captures not only supercell formation in small clusters but also, a plethora of published data from spreading tissues, like robust tension buildup in the center of the colony, the linear relationship between tensile stress and cell density (13), and the motion of cells around an uncoated surface area (16). We show that feedback between CIL, cell density, and cell–cell adhesion drives cells into a high-tension nonmotile state during tissue growth and spreading.

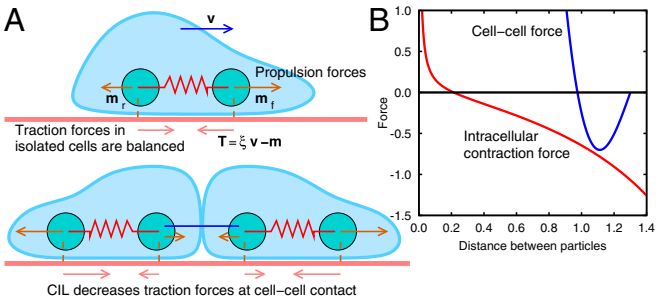

Fig. 1. Particle forces in the model simulation. (*A*) Schematic representation of model cells consisting of two particles. Front and rear particles exert propulsion forces of magnitudes m_f and m_r, respectively, on the substrate. On cell–cell contact, those forces change in magnitude and direction because of CIL (the text and *SI Text*). (*B*) Interparticle forces as a function of distance between particles. The red curve indicates intracellular force between particles of the same cell. The blue curve indicates interaction force for particles of different cells. The parameters for interaction forces where chosen according to the simulations in Fig. 3 (Table S1), with an assumed R_{cc} of 1.3 for the cell–cell adhesion force, corresponding to a cell length of $l = 1.0$ in simulation units.

Results

Key Mechanisms in the Model. In our simulation, every cell is represented by two particles. We assume that particle dynamics are overdamped because of strong adhesion to the substrate. We use a simple Euler scheme to update particle positions and calculate the velocity of each particle according to

$$\mathbf{v} = \frac{1}{\xi}\left(\mathbf{m} + \mathbf{f}_{\mathbf{contr}} + \mathbf{f}_{\mathbf{rep/adh}}\right),$$

with the coefficient of friction ξ.

Particles of the same cell interact by an attractive force $\mathbf{f}_{\mathbf{contr}}$ that increases with distance between the particles and models intracellular cytoskeletal contraction (Fig. 1 and *SI Text*). Contraction is balanced by "propulsion" force $\mathbf{m}$ that both particles exert on the substrate. For single cells in isolation, propulsion forces on both particles act along the cell axis and away from the cell center, accounting for a 1D representation of the traction force pattern of a single cell. Cell growth is mainly driven by those propulsion forces, because the intracellular force is only repulsive at very short distances to prevent particle overlap. In each cell, we distinguish front and rear particles, and if the magnitude of the propulsion force of the front particle m_f is larger than the propulsion force of the rear particle m_r, a single cell will experience a net motility force and move along its axis with a velocity $\mathbf{v}$. The traction force that each particle exerts on the substrate is then given by $\xi\mathbf{v} - \mathbf{m}$. Nonmotile cells are characterized by $m_f = m_r$ in our simulation and have a vanishing net motility force. In other words, both particles of a nonmotile cell are treated as rear particles.

The cells in our model can divide with a probability that depends on the cell size. It has been shown experimentally that a high cell density can impair cell division through contact inhibition of proliferation (41). Furthermore, it was shown that stretching of epithelial sheets can induce cell cycle progression (42). The idea that an optimal pressure for cell division, called homeostatic pressure, exists was postulated in theoretical studies (43). For simplicity, cells in our model divide with a given probability when their length l crosses a certain size threshold instead of changing the duration of the cell cycle with cell area. On division, two new particles are inserted.

The interaction force between particles of different cells $\mathbf{f}_{\mathbf{rep/adh}}$ is repulsive at short distances, modeling volume exclusion, and reaches a maximum attractive force f_{adh}^{max} at longer distances,

modeling cell–cell adhesion (Fig. 1 and *SI Text*). In the presence of other cells, the propulsion force **m** on each particle changes its direction and magnitude because of CIL. It aligns away from other particles in its vicinity, and the magnitude is additionally decreased according to the number of neighbors. For both motile and nonmotile cells, we calculate the sum of unit vectors connecting a particle at position $\mathbf{r}_i$ with its neighbors at positions $\mathbf{r}_j$, $\mathbf{R_i} = \sum_{j, r_{ij} < R_{inh}} \hat{\mathbf{r}}_{\mathbf{ij}}$, for each particle i. The propulsion force then reads $\mathbf{m} = -m_{f/r}\mathbf{R}/n$, where $m_{f/r}$ is a parameter, and n is the number of neighbor particles within the CIL range R_{inh}. Because cells can have variable lengths, both the range of the intercellular adhesion force and CIL are adjusted according to the cell size (*SI Text* and Fig. S1).

For the sake of completeness and compatibility with the earlier model version in ref. 27, we have also implemented a cell–cell alignment mechanism of cellular motility, in which the motility force of each cell tends to align with the average velocity (*SI Text*). To align with each other, cells switch between a motile state ($m_f > m_r$) and a nonmotile state ($m_f = m_r$). However, the difference in the magnitude of propulsion forces between front and rear particles for isolated motile cells is small compared with the changes in the propulsion force induced by CIL in both motile and nonmotile cells in our reference simulation (Table S1). Consequently, as we show below, this cell–cell alignment plays a relatively minor role for the effects discussed here.

We note that we do not use dissipative particle dynamics as in the model by Basan et al. (27), because we assume that substrate friction caused by adhesion is much stronger than inter- and intracellular friction. For simplicity, we do not include any Langevin forces; however, stochasticity in the system arises from switching between motile and nonmotile states for cell–cell alignment, and cell division. To calculate substrate traction stresses from particle traction forces, local averages within a range R_{trac} are taken. The intercellular stress is calculated from interparticle forces within a range R_h using the Hardy method (30).

Supercell Formation in Nonmotile Cell Clusters. Our model can be applied to nonmotile cells in a tissue. Isolated nonmotile cells in our simulation are characterized by $m_f = m_r$. When the cells assemble into a cluster, those propulsion forces are decreased according to our CIL mechanism. Single cells adhered to each other will have unbalanced substrate forces. We start our simulation with a very small cluster of four adhering cells and let the cluster grow by cell division (Fig. 2 and Movie S1). Our nonmotile cells exert forces on the substrate to balance intracellular contraction, and CIL leads to high outward-directed traction forces at the cluster edge and low traction forces in the center. Consequently, for small colonies, our results reproduce the experimentally observed supercell formation (Fig. 2 *E*–*G*). As the colony grows, the cell density becomes more heterogeneous, with the consequence that high propulsion forces are not only limited to the tissue edge but are locally observed in the tissue bulk as well (Fig. 2*H*). Especially after cell division, initially small cells have a small interaction range for CIL and therefore, exert high forces on the substrate until they have fully spread out (Fig. 2 *B* and *F*). Nonmotile supercells are generally under roughly uniform tension (Fig. 2 *I*–*L*); however, cell division can locally induce slight pressure (Fig. 2 *J* and *L*).

Supercell formation with traction forces only at the outer edge is experimentally observed for clusters of 2–30 cells (7–9). Traction forces in larger sheets have only been measured at relatively low resolutions (6, 11), but the results seem to agree with our model prediction that traction forces do not remain strictly limited to the edge in such clusters. We should also note that, although single cells are nonmotile, small colonies can move around or rotate because of CIL (Movie S1). CIL leads to imbalanced substrate forces in single cells, and asymmetric clusters can have imbalanced net edge forces. This phenomenon seems to mainly be an artifact from our simplified cell shape. As clusters grow, they tend to become more symmetric, and additionally, the total friction with the substrate increases, such that motion eventually stalls (ref. 35 has a detailed discussion of cluster motion). We conclude that, although we can show CIL and supercell formation in small clusters with our coarse-grained simulation, it is generally better suited for larger tissues, which we discuss below.

Expanding Cell Colony. To simulate a spreading colony, we seeded $N = 500$ motile cells in the center of our computational domain at a relatively low density. In comparison with our nonmotile cells discussed above, we increased the propulsion force of the front particle, decreased the maximum cell–cell adhesion force, and changed the parameters of the intracellular force toward a softer cell, such that cells can assume different lengths with only small variations in contraction. The cells start dividing, moving

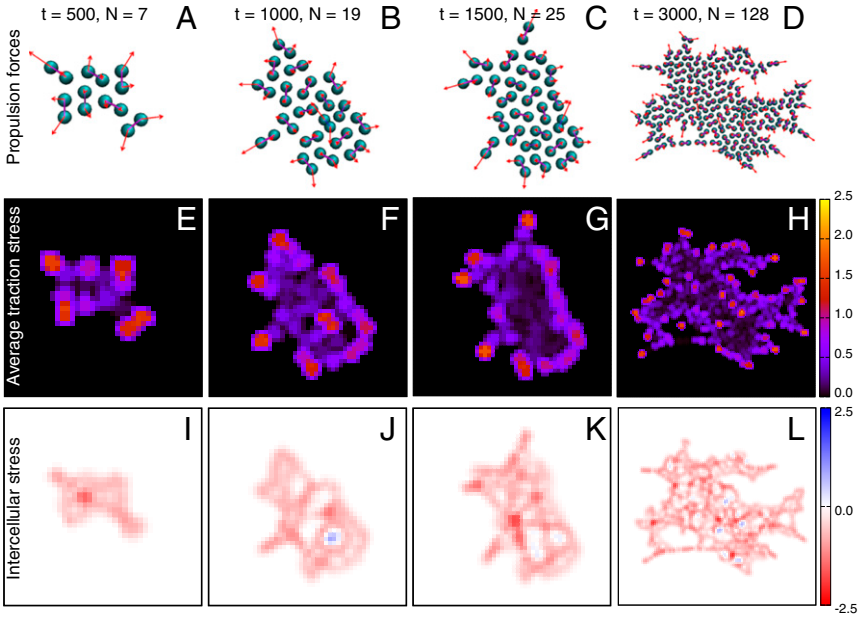

Fig. 2. Nonmotile cells in small clusters form supercells. Initially, four adhering cells are seeded on the substrate, and the cluster subsequently grows because of cell division. (*A*–*D*) Particles in the simulation at (*A*) $t = 500$, (*B*) $t = 1{,}000$, (*C*) $t = 1{,}500$, and (*D*) $t = 3{,}000$. Particles belonging to the same cell are additionally connected by thin lines, and the propulsion force m on each particle is shown as red arrows. N is the number of cells in the cluster. (*E*–*H*) Magnitude of traction forces exerted on the substrate. Forces within a distance $R_{trac} = 0.5$ of each grid point are locally averaged. (*I*–*L*) Average normal intercellular stress calculated with the Hardy method with $R_h = 1.0$ (30). Negative values (red) correspond to tension, and positive values (blue) correspond to pressure. Traction forces and intercellular stresses are both averaged over 100 time steps: $m_f = m_r = 1.3$, $f_{adh}^{max} = 1.4$, $f_{contr}^{0} = 0.1$, $R_{contr} = 1.0$, and $R_{div} = 0.85$. All other parameters are the same as in Table S1. All units are simulation units (Movie S1).

outward, and filling the available space. We calculated substrate traction stresses and intercellular stresses within the model tissue, and the results are shown in Fig. 3. In agreement with experimental data and in contrast to previous model versions (27, 30), stresses in the tissue are almost exclusively tensile because of the intracellular contraction force and CIL (Fig. S2). Moreover, tension increases from the tissue edge to the center (Fig. 3*C*). Traction stresses exerted by the tissue are heterogeneous (Fig. 3*B*); however, there is a bias toward the edges, which leads to the characteristic tension profile on integration along the x direction (Fig. 3*F*). The traction force pattern (Fig. 3*B*) and bell-shaped tension curve (Fig. 3*F*) are both in excellent agreement with experimental observations in a spreading MDCK cell colony (13).

We also see in our simulation that the cell density in the tissue center steadily increases as the colony expands (Fig. 3*D*). The same effect has been observed in the experiment (13, 41). Tension in the tissue follows the exact same trend, giving rise to a linear relationship between cell density and intercellular tension (Fig. 3*I*), again in excellent agreement with the experimental data (13). As the cell density increases toward the tissue center, the speed of outward migration of the cells decreases and eventually, drops to almost zero as the cell density crosses a threshold value (Fig. 3*H*). Cells in the tissue center experience kinetic arrest (41). An increase in cell speed toward the tissue edge has been measured experimentally in refs. 44 and 45. The relationship between cell speed and cell density (Fig. 3*H*) agrees well with the experimental data in ref. 46. We observe, consistent with the experiments in ref. 41, that CIL precedes contact inhibition of proliferation (i.e., the density continues to increase while the motion of cells has already stalled).

What is the feedback mechanism leading to a close coupling between cell density and intercellular tension? Contact inhibition aligns the propulsion forces of cells at the tissue edge away from the bulk, such that those cells "escape." Consequently, they reach a distance to their neighbors close to the maximum interaction distance (above the distance for maximal adhesion) and experience weak intercellular forces. At the same time, they make room for their followers, which also exert large propulsion forces, because the number of neighbors is low and CIL is weak. The ability to exert large propulsion forces, however, increases the cell length, leading to a lower cell density. As the number of neighbors increases, CIL decreases forces on the substrate. Therefore, cells cannot escape and get closer to their neighbors, and the cell–cell adhesion force tends to assume its maximum value, making it even less likely for cells to move away from their neighbors and driving them into a jammed state. Moreover, low propulsion forces entail small cells, and the density of adhesion force increases with cell density, leading to a higher intercellular tension.

We have verified this mechanism by changing some of our model parameters (Fig. S3). We ran a simulation without CIL, such that all cells always exert propulsion forces of given magnitude along the cell axis like individual cells, and cell–cell alignment is the dominant cause of tissue spreading (Fig. S3*A*). In that case, pressure instead of tension starts building up in the tissue center as the cell density increases. This behavior seems plausible, because cells continue to exert propulsion forces even at high cell densities and consequently, push against their neighbors. We can also vary the extent of CIL (*SI Text*). When lowering the level of CIL, stress in the tissue is tensile but does not increase toward the center (Fig. S3*B*). Hence, strong CIL is required for the tension buildup. When decreasing the maximum cell–cell adhesion force in our original simulation to a very low value, the tissue is under uniform low tension, whereas the density slightly increases over time, showing that increasing values of the cell–cell adhesion force determine the high tension in the tissue center (Fig. S3*D*). Moreover, the tissue spreads faster because of the lower cell density and weaker CIL. When decreasing the intracellular contraction parameter, the tissue is unable to support increasing tension at high cell density (Fig. S3*E*). When running a simulation without cell–cell alignment, the spreading velocity slightly decreases, but the tension buildup is undisturbed (Fig. S3*F*).

We next examined distributions of particle traction forces and velocities. We performed an analysis similar to that in ref. 13, where distributions of traction stresses were measured, and we calculated the distribution of the x component of instantaneous particle traction forces in a strip in the center of the tissue (Fig. 3*G*). At late stages of tissue spreading with high cell density, our traction force distribution agrees well with the measured data. It is broader than Gaussian and well-fitted by an exponential function. At the early stages of tissue growth, however, the

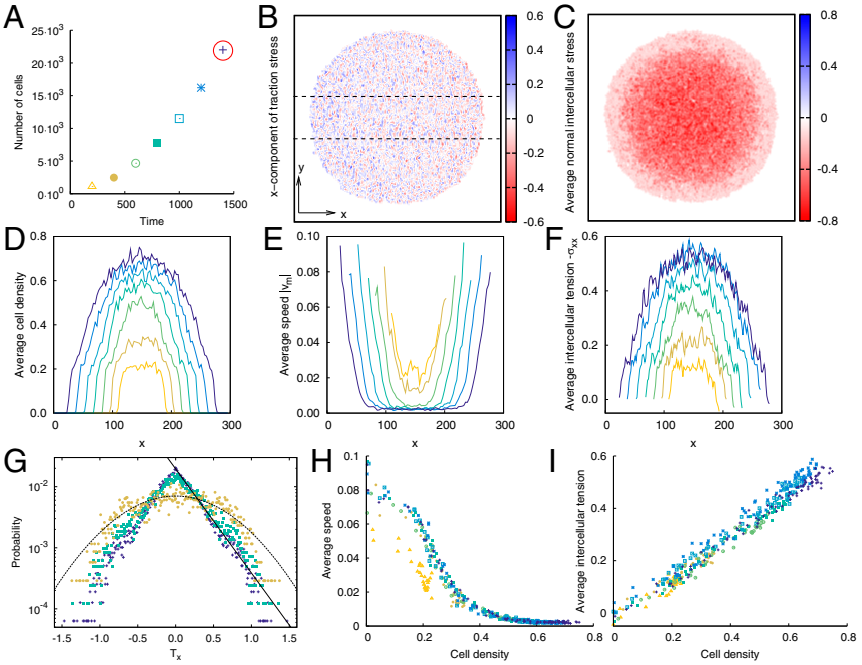

Fig. 3. Simulation of a spreading cell colony; $N = 500$ cells were seeded in the center of the computational domain at $t = 0$ and allowed to divide and migrate outward. (*A*) Total number of cells in the tissue at different time points. The red circle indicates that this simulation timeframe is shown in *B* and *C*. (*B*) Snapshot of the x component of the traction stress at $t = 1{,}400$ and $R_{trac} = 2.0$. (*C*) Average normal stress $(\sigma_{max} + \sigma_{min})/2$ calculated with the Hardy method (30) at $t = 1{,}400$ and $R_h = 2.0$. (*D*) Average cell density as a function of the x coordinate. (*E*) Average speed $|v_m|$ as a function of the x coordinate. The velocity is averaged over $t_{relax} = 50$. (*F*) Average tension in the x direction $-\sigma_{xx}$ calculated by integrating average traction stress T_x. In *D*–*F*, averages are taken along the y axis within the region indicated by dotted lines in *B*. (*G*) Distribution of the x component of particle traction forces within the region indicated in *B* for $t = 400$, $t = 800$, and $t = 1{,}400$ (colors). Exponential fit of the data for $t = 1{,}400$ (solid black line) and Gaussian fit of the data for $t = 400$ (dashed black line). (*H*) Average speed as a function of cell density. (*I*) Average tension as a function of cell density. Colors indicate data from different timeframes (*A*). Parameters are the same as in Table S1. All units are simulation units (Fig. S1 and Movie S2).

distribution is clearly narrower and rather well-fitted by a Gaussian curve. The peak in the distribution at $T_x = 0$ that develops over time is a signature of increasing effect of CIL in our model. As the cell density increases and consequently, CIL becomes more relevant, more particles will experience propulsion forces close to zero. Similarly, a peak around zero develops over time in the distribution of the x component of average particle velocity v_{mx} (Fig. S2). The distribution has broad tails caused by fast-moving cells at the tissue edge (Fig. S2*A*). When taking into account cells in the tissue interior only, the distribution is Gaussian, which is in agreement with the measured data in ref. 28. (Fig. S2*B*).

Obstacle Simulations. We also simulated a tissue moving around an uncoated circular substrate area where cells cannot adhere to the substrate (obstacle). In the simulation, the obstacle is modeled by setting the propulsion force $m_{f/r}$ to zero when particles enter the forbidden area. Similar to the behavior of the real tissue, cells move from the left to the right but do not enter the obstacle, although there is no hard wall, and only frictional forces and tension in the tissue counteract motion into the obstacle area (Fig. 4 *D* and *E* and Movie S3). The traction forces and velocities in the simulation (Fig. 4) agree rather well with experimental data (16). In particular, traction forces are always aligned toward the obstacle center at the obstacle boundary (Fig. 4 *A*–*C*), and there is no obvious correlation between the direction of traction stresses and the velocity. Although the traction force pattern agrees with the real tissue data at the immediate obstacle boundary, the alignment of traction forces at some distance from the obstacle is less pronounced in the simulation data, even when averaging over several simulations.

We also ran an obstacle simulation without CIL but motion dominated by cell–cell alignment instead (Movie S4). Interestingly, cells do not enclose the obstacle as smoothly as with CIL, because a wake forms behind the obstacle.

Discussion

We have performed model simulations for tissues consisting of motile or nonmotile cells to explore how cell–substrate and intercellular forces are generated in adhesive clusters and monolayers. Our model cells interact through CIL, meaning that contact with other cells decreases substrate forces, and propulsion forces align away from neighbors. CIL implies that cells at the edge of a tissue exert the strongest substrate traction forces. The fact that cells at the edge might behave differently from cells in the tissue interior was observed not only in cell clusters that form supercells (7–11) and spreading tissues experiencing kenotaxis (16) but also, with leader cells at the tip of fingers guiding the closure of model wounds (29, 47). Recently, it was shown that cell clusters consisting of nonchemotactic single cells can exhibit collective chemotaxis through CIL (33, 35, 48).

Simulations of spreading tissues exhibit remarkable agreement with experiments, particularly data on MDCK cells in refs. 13, 16, 41, and 46. Although cells at the edge of the spreading colony are highly motile, a high-tension nonmotile state emerges in the tissue interior as cells divide that is driven by a feedback between CIL, cell density, and cell–cell adhesion. Cells in our model always consisted of two particles. Therefore, we have implicitly assumed that the density of cell–cell adhesion sites increases with decreasing cell size. The cell–cell adhesion force, furthermore, varies with the distance between individual particles, giving rise to a linear relationship between cell density and tensile intercellular stress. Although closely packed cells in the tissue center experience high adhesion forces, cells at the edge exert only very weak forces on each other. Hence, cells at the edge do not physically pull their neighbors, and the mechanism for tension buildup in the center of the colony is not a tug-of-war mechanism (13) in the classical sense, which would mean that tension increases, because cells collectively pull outward and on each other. Our model rather suggests that motile cells at the tissue edge tend to move away from each other, which suppresses the formation of strong cell–cell adhesions, in contrast to cells in the tissue interior. We speculate that this high fluidity and low adhesion may also be required for a proper splitting of the tissue in front and motion around the circular obstacle. However, this mechanism does not seem to display extensive fingering at the edge of tissue as is sometimes observed (47). Whether fingering can be obtained by retuning the balance between adhesion and motion or whether it requires the addition of more complex biology (such as phenotypic differentiation into leader cells) needs to be addressed in future work. Stronger cell–cell adhesion may also play a role for the generation of stress waves during epithelial spreading (15).

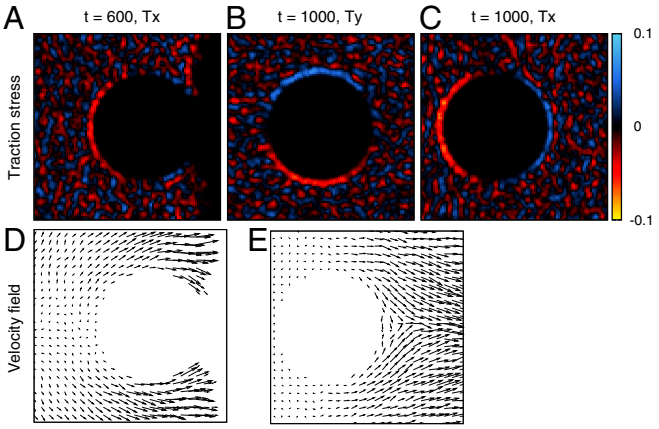

Fig. 4. Simulation of cells moving around an obstacle. Inability of cells to adhere on the circular obstacle is modeled by setting the propulsion force to zero when particles enter. (*A*) The x component of average traction stresses at $t = 600$. (*B*) The y component of average traction stresses at $t = 1{,}000$. (*C*) The x component of average traction stresses at $t = 1{,}000$. (*D*) Average velocity field at $t = 600$. (*E*) Average velocity field at $t = 1{,}000$. Averages are taken over five different simulations and for velocities, over a time $t_{relax} = 50$ each. The range for averaging traction stresses is $R_{trac} = 1.0$. The obstacle diameter (1 mm in the experiment in ref. 16) was chosen to be 30 simulation length units, which corresponds to about 30 typical cell sizes; $f_{adh}^{max} = 0.6$, and other parameters are the same as in Table S1. All units are simulation units (Movie S3).

The high-density region in the center of our spreading cell colony shows some characteristics of a jammed state. Jamming transitions have recently been argued to be of great importance for tissues (17, 22, 46). In ref. 13, the broad distribution of traction forces has been attributed to cell jamming. In agreement with that idea, the force distribution gets broader in our simulation as the cell density in the tissue center increases and cellular motility decreases. However, this distribution does not fully reflect the distribution of interparticle forces, which has been used to characterize jammed systems, such as a pile of sand. In fact, the cells in our model are not jammed in the sense that high cell density prohibits motile cells from moving, but rather, they actively down-regulate their propulsion forces in response to the density. This behavior, of course, is not possible in a nonliving system. Thus, the distribution of traction forces is a signature of increasing relevance of CIL in our model. In addition, the "jammed" state in our simulation exhibits strong cell–cell adhesions, in agreement with experimental observations on the spreading MDCK monolayer. In contrast, it has recently been suggested that lowering cell–cell adhesion forces leads to jamming in human bronchial epithelial cell layers (17).

Our model shows that traction forces of epithelia do not necessarily correlate directly with cellular motility but that cellular motion is, rather, a result of the complex interplay between intra- and intercellular as well as substrate forces. It has been suggested that cells

actively align their direction of migration in the direction of the intercellular stress in a process called "plithotaxis" (14, 49). In our model, the direction of principal stress is mainly determined by the cellular orientation, because intracellular contraction forces act along the cell axis. However, cells do not only move along their axis, because propulsion forces can be aligned in other directions because of our implementation of CIL. Hence, the cells in our model do not always exhibit plithotaxis. However, this fact may be a consequence of our simplified cell representation, and allowing cells to assume more complex shapes might be necessary to more carefully study the relationship between principal stress direction and velocity.

In conclusion, we have shown that inclusion of CIL enables us to create a particle-based model that can explain many experimental observations on nonmotile or motile cells organized in tissues. Our simulations suggest that the interaction between cell–substrate and cell–cell adhesion forces not only is responsible for supercell formation in small cell clusters but also, determines the behavior of extended layers of motile epithelial cells. Our model can robustly explain the predominance of tension in growing tissues and the surprising correlation between increasing density and increasing tensile forces.

ACKNOWLEDGMENTS. J.Z. thanks Jae Hun Kim for helpful discussions. This work was supported by National Science Foundation Grant DMS 1309542 and the Center for Theoretical Biological Physics. B.A.C. was supported by NIH Grant F32GM110983.

1. Dembo M, Wang YL (1999) Stresses at the cell-to-substrate interface during locomotion of fibroblasts. *Biophys J* 76(4):2307–2316.
2. Butler JP, Tolić-Nørrelykke IM, Fabry B, Fredberg JJ (2002) Traction fields, moments, and strain energy that cells exert on their surroundings. *Am J Physiol Cell Physiol* 282(3):C595–C605.
3. Reinhart-King CA, Dembo M, Hammer DA (2003) Endothelial cell traction forces on RGD-derivatized polyacrylamide substrata. *Langmuir* 19(5):1573–1579.
4. Sabass B, Gardel ML, Waterman CM, Schwarz US (2008) High resolution traction force microscopy based on experimental and computational advances. *Biophys J* 94(1): 207–220.
5. Ananthakrishnan R, Ehrlicher A (2007) The forces behind cell movement. *Int J Biol Sci* 3(5):303–317.
6. Saez A, et al. (2010) Traction forces exerted by epithelial cell sheets. *J Phys Condens Matter* 22(19):194119.
7. Maruthamuthu V, Sabass B, Schwarz US, Gardel ML (2011) Cell-ECM traction force modulates endogenous tension at cell-cell contacts. *Proc Natl Acad Sci USA* 108(12): 4708–4713.
8. Mertz AF, et al. (2012) Scaling of traction forces with the size of cohesive cell colonies. *Phys Rev Lett* 108(19):198101.
9. Mertz AF, et al. (2013) Cadherin-based intercellular adhesions organize epithelial cell-matrix traction forces. *Proc Natl Acad Sci USA* 110(3):842–847.
10. Ng MR, Besser A, Brugge JS, Danuser G (2014) Mapping the dynamics of force transduction at cell-cell junctions of epithelial clusters. *eLife* 3:e03282.
11. Ravasio A, et al. (2015) Regulation of epithelial cell organization by tuning cell-substrate adhesion. *Integr Biol (Camb)* 7(10):1228–1241.
12. du Roure O, et al. (2005) Force mapping in epithelial cell migration. *Proc Natl Acad Sci USA* 102(7):2390–2395.
13. Trepat X, et al. (2009) Physical forces during collective cell migration. *Nat Phys* 5(6): 426–430.
14. Tambe DT, et al. (2011) Collective cell guidance by cooperative intercellular forces. *Nat Mater* 10(6):469–475.
15. Serra-Picamal X, et al. (2012) Mechanical waves during tissue expansion. *Nat Phys* 8(8): 628–634.
16. Kim JH, et al. (2013) Propulsion and navigation within the advancing monolayer sheet. *Nat Mater* 12(9):856–863.
17. Park J-A, et al. (2015) Unjamming and cell shape in the asthmatic airway epithelium. *Nat Mater* 14(10):1040–1048.
18. Köpf MH, Pismen LM (2013) A continuum model of epithelial spreading. *Soft Matter* 9(14):3727–3734.
19. Banerjee S, Utuje KJC, Marchetti MC (2015) Propagating stress waves during epithelial expansion. *Phys Rev Lett* 114(22):228101.
20. Farhadifar R, Röper J-C, Aigouy B, Eaton S, Jülicher F (2007) The influence of cell mechanics, cell-cell interactions, and proliferation on epithelial packing. *Curr Biol* 17(24):2095–2104.
21. Kabla AJ (2012) Collective cell migration: Leadership, invasion and segregation. *J R Soc Interface* 9(77):3268–3278.
22. Bi D, Yang X, Marchetti MC, Manning ML (2015) Motility-driven glass and jamming transitions in biological tissues. arXiv:1509.06578.
23. Camley BA, et al. (2014) Polarity mechanisms such as contact inhibition of locomotion regulate persistent rotational motion of mammalian cells on micropatterns. *Proc Natl Acad Sci USA* 111(41):14770–14775.
24. Löber J, Ziebert F, Aranson IS (2015) Collisions of deformable cells lead to collective migration. *Sci Rep* 5:9172.
25. Palmieri B, Bresler Y, Wirtz D, Grant M (2015) Multiple scale model for cell migration in monolayers: Elastic mismatch between cells enhances motility. *Sci Rep* 5:11745.
26. Szabó B, et al. (2006) Phase transition in the collective migration of tissue cells: Experiment and model. *Phys Rev E Stat Nonlin Soft Matter Phys* 74(6 Pt 1):061908.
27. Basan M, Elgeti J, Hannezo E, Rappel W-J, Levine H (2013) Alignment of cellular motility forces with tissue flow as a mechanism for efficient wound healing. *Proc Natl Acad Sci USA* 110(7):2452–2459.
28. Sepúlveda N, et al. (2013) Collective cell motion in an epithelial sheet can be quantitatively described by a stochastic interacting particle model. *PLOS Comput Biol* 9(3): e1002944.
29. Tarle V, Ravasio A, Hakim V, Gov NS (2015) Modeling the finger instability in an expanding cell monolayer. *Integr Biol (Camb)* 7(10):1218–1227.
30. Zimmermann J, et al. (2014) Intercellular stress reconstitution from traction force data. *Biophys J* 107(3):548–554.
31. Loeb L (1921) Ameboid movement, tissue formation and consistency of protoplasm. *Am J Physiol* 56(1):140–167.
32. Abercrombie M, Heaysman JEM (1953) Observations on the social behaviour of cells in tissue culture. I. Speed of movement of chick heart fibroblasts in relation to their mutual contacts. *Exp Cell Res* 5(1):111–131.
33. Theveneau E, et al. (2010) Collective chemotaxis requires contact-dependent cell polarity. *Dev Cell* 19(1):39–53.
34. Lin B, Yin T, Wu YI, Inoue T, Levchenko A (2015) Interplay between chemotaxis and contact inhibition of locomotion determines exploratory cell migration. *Nat Commun* 6:6619.
35. Camley BA, Zimmermann J, Levine H, Rappel W-J (2015) Emergent collective chemotaxis without single-cell gradient sensing. arXiv:1506.06698.
36. Mayor R, Carmona-Fontaine C (2010) Keeping in touch with contact inhibition of locomotion. *Trends Cell Biol* 20(6):319–328.
37. Carmona-Fontaine C, et al. (2008) Contact inhibition of locomotion in vivo controls neural crest directional migration. *Nature* 456(7224):957–961.
38. Astin JW, et al. (2010) Competition amongst Eph receptors regulates contact inhibition of locomotion and invasiveness in prostate cancer cells. *Nat Cell Biol* 12(12): 1194–1204.
39. Yamada S, Nelson WJ (2007) Localized zones of Rho and Rac activities drive initiation and expansion of epithelial cell-cell adhesion. *J Cell Biol* 178(3):517–527.
40. Rørth P (2012) Fellow travellers: Emergent properties of collective cell migration. *EMBO Rep* 13(11):984–991.
41. Puliafito A, et al. (2012) Collective and single cell behavior in epithelial contact inhibition. *Proc Natl Acad Sci USA* 109(3):739–744.
42. Streichan SJ, Hoerner CR, Schneidt T, Holzer D, Hufnagel L (2014) Spatial constraints control cell proliferation in tissues. *Proc Natl Acad Sci USA* 111(15):5586–5591.
43. Podewitz N, Delarue M, Elgeti J (2015) Tissue homeostasis: A tensile state. *Europhys Lett* 109(5):58005.
44. Lee RM, Kelley DH, Nordstrom KN, Ouellette NT, Losert W (2013) Quantifying stretching and rearrangement in epithelial sheet migration. *New J Phys* 15(2):025036.
45. Nnetu KD, Knorr M, Strehle D, Zink M, Käs JA (2012) Directed persistent motion maintains sheet integrity during multi-cellular spreading and migration. *Soft Matter* 8(26):6913–6921.
46. Angelini TE, et al. (2011) Glass-like dynamics of collective cell migration. *Proc Natl Acad Sci USA* 108(12):4714–4719.
47. Reffay M, et al. (2014) Interplay of RhoA and mechanical forces in collective cell migration driven by leader cells. *Nat Cell Biol* 16(3):217–223.
48. Camley BA, Zimmermann J, Levine H, Rappel W-J (2015) Collective signal processing in cluster chemotaxis: Roles of adaptation, amplification, and co-attraction in collective guidance. arXiv:1512.00544.
49. Das T, et al. (2015) A molecular mechanotransduction pathway regulates collective migration of epithelial cells. *Nat Cell Biol* 17(3):276–287.